

1
2
3
4
5
6
7
8
9
10
11
12
13
14
15
16
17
18
19
20
21
22
23
24
25
26
27

Revision 2

Title:

Aluminum speeds up the hydrothermal alteration of olivine

Muriel Andreani, Isabelle Daniel, Marion Pollet-Villard

Laboratoire de Géologie de Lyon : Terre, Planètes, Environnement, UMR 5276
CNRS, Université Claude Bernard et Ecole Normale Supérieure de Lyon,
2 rue Raphael Dubois,
69622 Villeurbanne
France

Corresponding author: muriel.andreani@univ-lyon1.fr

28 **Abstract**

29

30 The reactivity of ultramafic rocks under hydrothermal conditions controls chemical
31 fluxes at the interface between the internal and external reservoirs of silicate planets. On
32 Earth, hydration of ultramafic rocks is ubiquitous and operates from deep subduction
33 zones to shallow lithospheric environments where it considerably affects the physical
34 and chemical properties of rocks and can interact with the biosphere. This process also
35 has key emerging societal implications, such as the production of hydrogen as a source
36 of carbon-free energy. To date, the chemical model systems used to reproduce olivine
37 hydrothermal alteration lead to the formation of serpentine with sluggish reaction rates.
38 Here, we use in situ diamond anvil cell experiments and show that the presence of
39 aluminum in hydrothermal fluids increases the rate of olivine serpentinization by one to
40 two orders of magnitude. Aluminum increases the solubility of olivine and enhances the
41 precipitation of aluminous serpentine. After two days, olivine crystals were fully
42 transformed to aluminous serpentine under conditions typical of natural hydrothermal
43 environments, i.e., 200°C and 300°C, 200 MPa. This result motivates a re-evaluation of
44 the natural rates of olivine serpentinization and of olivine hydrolysis in general in a wide
45 range of settings. This discovery also opens the potential of the serpentinization reaction
46 for industrial scale production of hydrogen at economically feasible timescales and
47 temperature.

48

49 **Keywords:** olivine, hydrothermal, serpentinization, aluminium

50 **1) Introduction**

51

52 The hydrothermal alteration of olivine is a widespread process that occurs in many
53 geological settings wherever warm aqueous fluids react with ultramafic mantle rocks or
54 olivine-rich magmatic rocks (e.g. wherlite, troctolites, gabbros). Most of the time, olivine
55 is transformed into the hydrous sheet silicate serpentine, plus variable amounts of iron
56 oxides and magnesium hydroxides as illustrated by the olivine serpentinization
57 reaction:



59 olivine (Fo₉₀) Mg-serpentine brucite magnetite

60 If the system chemistry differs from that locally imposed by olivine, the hydrated
61 product minerals can differ. A silica input from either dissolving neighbouring minerals
62 or the hydrothermal fluid would inhibit brucite formation, and even lead to talc
63 precipitation for higher Si activity. Chlorite and tremolite may also form at olivine-
64 plagioclase contact within olivine-rich magmatic rocks. Talc-chlorite-tremolite-
65 serpentine is actually observed within oceanic detachment faults as a result of Si-Al-Ca
66 metasomatism by fluid arising from distant mafic units (Boschi et al. 2006; Jons et al.
67 2010).

68

69 The hydrothermal alteration of olivine (e.g. Eq1) presents several fundamental and
70 societal implications. It alters the physical, mechanical and chemical properties of
71 ultramafic rocks and it is accompanied by a redox reaction producing hydrogen coupled
72 to reduction of water and oxidation of olivine ferrous component. The ferric iron is
73 integrated into iron oxides and/or into the hydrous phase. Indeed, chlorite and
74 serpentine can both incorporate important amounts of ferric iron in their structure (e.g.

75 O'Hanley and Dyar 1993; Muñoz et al. 2006; Andreani et al. 2013). Hydrogen, resulting
76 from serpentine and/or chlorite formation, has been identified within fluids venting at
77 ultramafic-hosted hydrothermal sites along mid-ocean ridges (Charlou et al. 2002;
78 Seyfried et al. 2011) as well as in experiments performed in large-volume reactor (Allen
79 and Seyfried 2003; Seyfried et al. 2007; Marcaillou et al. 2011). Production of abiotic H₂
80 is also thermodynamically predicted using reaction path modelling (Klein et al. 2009). It
81 provides a source of metabolic energy for deep chemoautotrophic ecosystems and could
82 also act as an industrial-scale energy source. In the presence of CO₂, the availability of
83 molecular hydrogen also controls the balance between CO₂-mineralisation and abiotic
84 CO₂-reduction, including Fischer Tropsch-type reactions (McCollom and Seewald 2007;
85 Proskurowski et al. 2008). Ultramafic-hosted hydrothermal systems have thus been
86 proposed as a site for the emergence of the earliest ecosystems (Martin et al. 2008), as
87 well as for CO₂ storage and remediation both at industrial and geological time scales
88 (Kelemen and Matter 2008; Nakamura and Kato 2004; Andreani et al. 2009).

89 Serpentinized or metasomatized ultramafic rocks are common in the oceanic
90 lithosphere particularly along slow and ultra-slow spreading ridges (Cannat, 1993), in
91 subduction zones within and above the downgoing slab (Peacock 1990; Reynard et al.
92 2007), along active continental faults (Andreani et al. 2005; Solum et al. 2006) and
93 within Archean supracrustal terranes (Blais and Auvray 1990; Arndt et al. 2008). In
94 extraterrestrial environments, serpentines have been identified in meteorites (Tomeoka
95 and Tanimura 2000), and on the surface of Mars together with chlorite (Ehlmann et al.
96 2010). The presence of serpentine has also been hypothesized in the core of icy satellites
97 like Titan (Choukroun et al. 2010).

98

99 Despite the ubiquity of fully to partially altered olivine in nature, the thermochemical
100 conditions and kinetics of this combined hydration and redox reaction are not yet well
101 established. Serpentine as a result of olivine hydration is widespread. The stability field
102 of serpentine in the MgO-SiO₂-H₂O (MSH) system extends up to a maximum temperature
103 of 730°C at 2.1 GPa, i.e., the invariant point of the dehydration curve of antigorite. At
104 lower pressure (< 1 GPa) the stability field of serpentine is enlarged toward high
105 temperature as a function of Al content in the MgO-Al₂O₃-SiO₂-H₂O (MASH) system
106 (O'Hanley 1996). Serpentinization is active at T < 150°C near ridge axes (Proskurowski
107 et al. 2006), and is suspected at even lower temperature within ophiolites (Barnes and
108 O'Neil 1978). Experimental studies have reproduced the serpentinization reaction of
109 olivine, pyroxene or bulk peridotite at temperatures between 188 and 560°C, and
110 pressures from 20 to 300 MPa (e.g. Allen and Seyfried 2003; Seyfried et al. 2007;
111 Marcaillou et al. 2011, McCollom and Seewald 2007; Martin and Fyfe 1970; Wegner and
112 Ernst 1983; Luquot et al. 2010). These experiments were performed in either pure
113 water or an aqueous fluid closer to seawater composition. They have mostly focused on
114 the chemical evolution of the fluid phase or on the rate of gas or organic compound
115 production. Serpentinization rates were measured in four of these studies only and were
116 found to be very low (Martin and Fyfe 1970; Wegner and Ernst 1983; Luquot et al. 2010;
117 Marcaillou et al. 2011). None of the above-mentioned experiments has used an aqueous
118 fluid with a seawater-modified chemistry, as expected in open natural settings, e.g. after
119 it has interacted with magmatic units or sediments. Although aluminum is one
120 of the common elements associated with the metasomatism of ultramafic rocks (e.g.
121 Boschi et al. 2006; Jons et al. 2010), its role in the hydrolysis of olivine has only been
122 investigated at low pH (2 < pH < 5) and low T conditions, T=65° (Chen and Brantley
123 2000). This is probably due to the fact that aluminum is often considered as an immobile

124 element because of the very low solubility of aluminous minerals in pure water.
125 Nevertheless, several studies of metamorphic rocks describing ubiquitous Al-bearing
126 mineralization in veins have highlighted the mobility of Al within fluids (e.g. Kerrick
127 1990). Experimental works have also shown that the presence of Si or Na in solution
128 leads to the formation of Si-Al or Na-Al complexes respectively, for pH >4 to 5 (Diakonov
129 et al. 1996; Manning 2006). This complexation considerably enhances the solubility of
130 alumino-silicates and the mobility of aluminum in metamorphic or metasomatic fluids
131 despite current thoughts on the low solubility of corundum in pure water (Manning
132 2007). Moreover, abundant aluminum supply exceeding provision by pyroxenes in
133 ultramafic rocks is expected in fluids released from the dehydration of metapelites in
134 subduction zones as well as during the hydrothermal alteration of gabbros at mid-ocean
135 ridges. Aluminum was also abundant in primitive environments of both the Earth and
136 Mars, stored in either Al-rich minerals like plagioclase or Al-enriched ultramafic lavas
137 like Munro-type or other high Al₂O₃/TiO₂ komatiites (Arndt et al. 2008).
138 In order to investigate the influence of Al on the hydrothermal alteration of olivine in
139 those contexts, we have performed a series of experiments using a low-pressure
140 diamond anvil cell (lp-DAC, Supporting Figure S1 and Oger et al. 2005) under P-T
141 conditions representative of lower crust while following the reaction progress in situ by
142 optical imaging and by confocal Raman spectroscopy.

143

144 **2) Methods**

145 Temperature in the low-pressure diamond anvil cell (lp-DAC, Supporting Figure S1) was
146 monitored with a thermocouple in contact with the gasket. Aluminum was introduced
147 either as a gel of aluminum hydroxide formed by reaction of AlCl₃ with water and
148 sodium hydroxide for experiments run at 200°C (pH set at 7, at 25°C), or as Al₂O₃ ruby

149 microspheres for experiments run at 300°C (pH measured at 25°C = 6.8). The most
150 appropriate source of aluminum has been used for the two different temperatures in
151 order to always ensure an excess of aluminum in the fluid and keep similar cations in the
152 initial fluid for all experiments. Indeed, the reactivity and dissolution kinetics of Al₂O₃ in
153 a 0.5 m NaCl aqueous fluid was tested separately in a temperature-step experiment,
154 which showed an almost instantaneous dissolution of Al₂O₃ microspheres at a
155 temperature above 280°C only. Therefore, another source of Al, minimizing chemical
156 changes, has thus been chosen for the 200°C experiments. Al₂O₃ ruby microspheres also
157 allowed pressure measurement and pressure cell calibration. Pressure was set and
158 maintained constant throughout experiments by having a tight control of the gas
159 membrane pressure of the lp-DAC. The sample was sealed with a Ni-gasket lined with
160 gold to prevent reaction between the sample chamber and the gasket. Dimensions of the
161 reacting cell are 380 μm in diameter and 300 μm thickness (Figure S1).
162 The progress of reaction was monitored by optical microscopy and confocal Raman
163 microspectrometry using a Horiba Jobin-Yvon LabRAM HR800 Raman spectrometer at
164 the ENS (Lyon, France) using green laser at 514 cm⁻¹ with a beam size of ~3 μm.
165 X-Ray Diffraction (XRD) spectra have been acquired under an angle-dispersive mode
166 using a monochromatic radiation (33 keV, λ=0.3738 Å), focused into a spot of 8x8 μm in
167 size.

168

169 **3) Experimental results**

170

171 Experiments were run for 4.5 to 7.5 days with two olivine (Ol) grains reacted in saline
172 water (0.5 mol NaCl /kg) at 200°C and 300°C, and P=200 ±30 MPa. To ensure an excess
173 of Al in the fluid under the experimental conditions, aluminum was introduced either as

174 a gel of aluminum hydroxide for experiments at 200°C, or as Al₂O₃ ruby microspheres
175 for experiments at 300°C. The importance of nucleation in the kinetics of olivine
176 serpentinization has also been tested by adding lizardite (Mg-serpentine) nuclei in a
177 subset of experimental runs. Table 1 summarizes the experimental conditions and main
178 results of the experiments reported hereafter.

179

180 Aluminum-free experiments N°1 and N°2 do not show any visible reaction progress
181 even after one-week duration, whereas reaction starts rapidly when Al is added to the
182 system in experiments N°3 and N°4 at 300°C and in experiments N°5 and N°6 at 200°C.
183 The first grains of reaction products appear on olivine within 2 hours (Table 1) in the
184 absence of lizardite nuclei and the reaction goes to completion in 2 days. The
185 progressive coating of initially transparent olivine and Al₂O₃ microspheres by brown
186 crystals is illustrated in Figure 1. Figure 2 shows the corresponding evolution of the
187 Raman spectra of olivine with time. It indicates the total disappearance of olivine after
188 t=47h, that is confirmed by the XRD characterization of final reaction products (Figure
189 3C). The softness of the material noticed during its extraction from the lp-DAC also
190 confirms the absence of any relict of olivine crystal in the core of the aggregate and the
191 completion of the reaction. Figure 3A and 3B show the ghost olivine grain fully replaced
192 by micrometric grains of a sheet silicate enriched in aluminum as evidenced by EDS-SEM
193 analyses. X-Ray Diffraction shows that this silicate belongs to the serpentine group of
194 minerals (Figure 3C). It was identified as the Al-rich serpentine amesite by Raman
195 spectroscopy (Figure 2) in all the Al-bearing experiments void of lizardite nuclei (Exp.
196 N°3a, 3b, 5, and 6). Serpentine is the only reaction product observed. Magnetite or
197 brucite predicted by equation 1 for a pure MSH system have not been detected. The
198 serpentine grains are enriched in iron and accommodate the iron released from olivine.

199 The very fast precipitation of Al-rich serpentine may inhibit magnetite nucleation here.
200 However, this does not rule out the H₂ production since serpentines classically
201 incorporate non negligible amount of ferric iron in their structure that contributes to H₂
202 production (e.g. O'Hanley and Dyar 1993; Marcaillou et al. 2011; Andreani et al. 2013).
203 Unfortunately, H₂ could not be detected in situ since expected concentrations in the fluid
204 are below detection limit by Raman spectroscopy. Indirect estimation of H₂ by
205 quantifying the ferric iron in microscopic serpentine using synchrotron-based X-ray
206 absorption was beyond the scope of this work. When lizardite nuclei are added to the
207 starting materials at 300°C (Exp. N° 4), new serpentine grains formed after 1.5 days
208 (Supporting Figure S2) with a chemical composition and Raman spectra close to that of
209 the lizardite nuclei. The reaction, however, did not go to completion during the duration
210 of the experiment. We documented a fast partial transformation of olivine into
211 serpentine visible over 3 days and the reaction stopped or slowed down to a rate that
212 precluded further observation. The latter experiment illustrates the importance of
213 removing Al from the fluid or from the reactive interface in order to continue the
214 reaction. Experiment N°3b includes a first temperature step at 250°C for 3 days followed
215 by a second and final step of 300°C for 6 days. The latter experiment confirms that the
216 Al₂O₃ microspheres do not dissolve at 250°C and that, as a consequence, the
217 serpentinization reaction fails to start. Optical observations demonstrate that the onset
218 of serpentinization is correlated with the dissolution of Al₂O₃ microspheres at 300°C and
219 that the first grains of serpentine appear simultaneously on the surface of both olivine
220 grains and Al₂O₃ microspheres (Figure 1B). This supports the critical role of dissolved Al
221 to speed up both the dissolution kinetics of olivine and the nucleation and growth of Al-
222 rich serpentine. It also demonstrates that olivine dissolution is the limiting parameter of

223 the serpentinization reaction and that olivine solubility is considerably enhanced by the
224 presence of dissolved Al in the fluid.

225

226 **4) Mutually enhanced dissolution of olivine and alumina**

227

228 Since Al is not a major component of olivine, it was not expected to directly control
229 olivine's solubility. At 300°C, 86 bars in aqueous solution, Salvi et al. (1998) nevertheless
230 found that $\text{Al}(\text{OH})_3(\text{H}_3\text{SiO}_4)^-$ is the dominant aluminous silica species at $\text{pH} < 2$ and $\text{pH} >$
231 4.5. They also observed that the formation of Al-Si complexes increases the solubility of
232 some aluminosilicates or oxide minerals such as kaolinite or boehmite, similar to that
233 was observed at higher P-T conditions (Manning, 2007). Under the conditions of the
234 present experiments, the best pH estimate is 6 at $T = 300^\circ\text{C}$ (CHESS code (Van der Lee et
235 al. 2002)). Thus, dissolved Al in our experiments should be complexed to the Si released
236 by dissolving olivine (Salvi et al. 1998). This may be responsible for the observed
237 increase in olivine solubility in our Al-bearing experiments and the fast serpentine
238 precipitation. Such a mutually enhanced dissolution of olivine and alumina leads to the
239 precipitation of amesite under the present experimental conditions (Figure 3) but may
240 also lead to the formation of other Al-rich hydrated silicate, like chlorite for instance,
241 under slightly different chemical conditions. When lizardite is initially present in the
242 system (Exp. N°4), aluminum still accelerates olivine dissolution. Serpentine growth
243 starts on olivine as well as on available lizardite nuclei which leads to a more magnesian
244 chemical composition of the newly formed serpentine. This slows down the reaction
245 since the Al released by the alumina microspheres is less efficiently removed from the
246 solution by serpentine precipitation. Thus, the equilibrium solubility of alumina under
247 those conditions is more rapidly reached. This effect certainly does not apply to open

248 natural systems where local chemical gradients and fluid renewal at mineral interface
249 are expected to refresh the fluid and thus remove excess Al from the reacting zone.
250 The results of experiments N°3a, 3b, 5 and 6 are compared in Figure 4 to those of the Al-
251 free experiment N°1 and to previously published serpentinization rates of olivine
252 (Martin and Fyfe 1970; Wegner and Ernst 1983; Luquot et al. 2010) and of peridotite
253 (Marcaillou et al. 2011). Assuming a linear conversion rate of olivine into serpentine, we
254 obtain a mean serpentinisation rate of 49 % per day in the present study. This is c.a. 7 to
255 50 times higher than the rates reported under very similar conditions (3.7 - 7.5 % per
256 day (Martin and Fyfe 1970); 1 - 3 %/day (Wegner and Ernst 1983)). It is also 30 to 50
257 times higher than the rates of 1-2 % /day reported for peridotite at lower pressure (P =
258 30 MPa) with a smaller grain size of 1 μm (Marcaillou et al. 2011). The latter work also
259 shows that after 77% of serpentinization the conversion rate decreases down to 0.3
260 %/day and approaches that reported at 200°C, 20 MPa during dynamic percolation
261 experiments which was of 0.2-0.4%/day (Luquot et al. 2010); i.e. two orders of
262 magnitude lower than those in the Al-bearing experiment reported here.

263

264 **5) Implications**

265

266 In natural open systems where a sustained H₂O flow allows hydration reactions, the rate
267 of olivine alteration may be increased at any time depending on the inlet fluid flux and
268 its Al content. Indeed, Al is always present in variable amount in serpentine minerals
269 ranging from 1 to 27 wt. % of Al₂O₃ (O'Hanley 1996; Beard et al. 2009), and it is a major
270 component of chlorite. Consequently our experimental results suggest that the
271 hydrothermal alteration of olivine is probably much faster in natural settings where
272 peridotites are intimately associated with Al-suppliers such as the common magmatic

273 bodies in slow-spreading oceanic crust (Cannat 1993). This is actually well illustrated at
274 oceanic detachments where fault material results from peridotite-gabbro metasomatism
275 and where active hydrothermal fields are observed (McCaig et al. 2007). The
276 composition of fluids released at these hydrothermal vents is enriched in H₂, CH₄ and
277 complex organic compounds and is mainly controlled by serpentinization at depth. The
278 local abundance of Al issued from magmatic rocks certainly affects the fluxes of products
279 released during serpentinization, and in consequence the development of the ecosystem
280 associated with these hydrothermal fields (Schrenk et al. 2004). The effect of joined
281 alteration of olivine and Al-bearing mineral, like plagioclase, on H₂ production in a
282 natural system has indeed been described by Seyfried et al. (2011), based on the
283 chemistry of the fluids that escape the Rainbow hydrothermal field (36°N, Mid-Atlantic
284 Ridge).

285

286 The effect of Al on lower crust and upper mantle metamorphism and metasomatism is
287 expected to be even stronger at high pressure in subduction zones where those
288 reactions control the rheology and physical properties of the subducting plate and
289 mantle wedge (Peacock and Hyndman 1999; Reynard et al. 2007). Indeed, the solubility
290 of Al related to the stability of Na-Si-Al complexes in solution is greater at high pressure
291 (Manning 2007), and may exceed the solubility of Mg or Fe in fluids equilibrated with
292 mafic and felsic bulk compositions (Manning 2006).

293

294 Whatever the setting, the rate of metamorphic reaction is also a key parameter for
295 determining the contribution of reaction-enhanced processes at the micrometer-scale,
296 such as reaction-driven cracking, that can affect, in turn, macroscopic rock properties
297 like permeability (Jamveit et al. 2008; Rudge et al. 2010). Reaction-driven cracking has

298 been proposed as an important positive feedback of the olivine hydration reaction that
299 creates permeability for fluid supply and increases the reactive surface area (Kelemen
300 and Hirth 2012). A well documented example is the case of fractured plagioclase grains
301 between serpentinized or chloritized olivine crystals in troctolites or olivine gabbros,
302 respectively. The present results suggest that the presence of Al in solution should, at
303 least locally, increase the contribution of reaction-induced cracking during retrograde
304 metamorphism of olivine-rich rocks.

305

306 The present results also provide a way to accelerate serpentinization reactions towards
307 an economically feasible time-scale for industrial H₂ production and/or CO₂ remediation
308 through the production of carbon compounds with a higher added value like CH₄ and
309 hydrocarbons. In comparison with available technologies for H₂ production that mainly
310 rely on fossil fuels (> 90% of H₂ production by steam reforming and < 1% via
311 electrolysis), olivine serpentinization is a carbon-free process. Energy minimization is
312 also obtained here by the exothermic character of the serpentinization reaction and by
313 lowering the temperature of the reaction to 200°C, as long as Al is available in solution.

314

315 **6) Acknowledgments**

316

317 The authors thank Bertrand Van de Moortèle for performing SEM imaging supported by
318 the CLYM (Lyon University, France), and Hervé Cardon and Gilles Montagnac for their
319 assistance during HP experiments and Raman spectroscopy at the Ecole Normale
320 Supérieure de Lyon. Raman spectroscopy is supported by the Institut National des
321 Sciences de l'Univers. We also want to thank M. Godard, S. Mojziz, and B. Reynard for
322 discussion and comments on the manuscript. This work was supported by the

323 Programme Interdisciplinaire Energie of the CNRS (to MA) and by the Institut
324 Universitaire de France (to ID).

325

326

327 **References**

328

329 Allen, D.E and Seyfried, W. E. (2003), Compositional controls on vent fluids from
330 ultramafic-hosted hydrothermal systems at mid-ocean ridges: An experimental study at
331 400 °C, 500 bars, *Geochimica et Cosmochimica Acta*, 67, 1531-1542.

332

333 Andreani, M., Boullier, A-M., Gratier, J-P. (2005) Development of schistosity by
334 dissolution-crystallization in a californian serpentinite gouge. *Journal of Structural*
335 *Geology*, 27, 2256-2267

336

337 Andreani, M., Luquot, L., Gouze, P, Godard, M., Hoisé, E., Gibert, B. (2009) Experimental
338 study of carbon sequestration reactions controlled by the percolation of CO₂-rich brine
339 through peridotites. *Environmental Science and Technology*, 43, 1226-1231

340

341 Andreani, M., Muñoz, M., Marcaillou, C., Delacour, A. (2013) μ XANES study of iron redox
342 state in serpentine during oceanic serpentinization. *Lithos*, in press.

343

344 Arndt, N., Lescher, C.M., Barnes, S.J., (2008) *Komatiite*. Cambridge University Press, New
345 York, 488 p.

346

347 Barnes, I., O'Neil, J.R. (1978) Present-day serpentinization in New Caledonia, Oman and
348 Yugoslavia. *Geochimica et Cosmochimica Acta*, 42, 144-145.

349

350 Beard, J.S., Frost, B.R., Fryer, P., McCaig, A., Searle, R., Ildefonse, B., Zinin, P., Sharma, S.K.
351 (2009) Onset and progression of serpentinization and magnetite formation in olivine-
352 rich troctolite from IODP hole U1309D. *Journal of Petrology*, 50, 387-403.

353

- 354 Blais, S. and Auvray, B., (1990) Serpentinization in the archean komatiitic rocks of the
355 Kuhmo greenstone belt, Eastern Finland. *Canadian Mineralogist*, 28.
356
- 357 Boschi, C., Früh-Green, G.L., Delacour, A., Karson, J., Kelley, D. (2006) Mass transfer and
358 fluid flow during detachment faulting and development of an oceanic core complex,
359 Atlantis Massif (MAR 30°N). *Geochemistry Geophysics Geosystems*, 7, Q01004.
360
- 361 Cannat, M. (1993) Emplacement of mantle rocks in the seafloor at Mid-Atlantic Ridges.
362 *Journal of Geophysical Research*, 98, 4163-4172.
363
- 364 Charlou, J-L., Donval, J-P., Fouquet, Jean-Baptiste, A., Holm, N. (2002) Geochemistry of
365 high H₂ and CH₄ vent fluids issuing from ultramafic rocks at the Rainbow hydrothermal
366 field (36°14'N, MAR). *Chemical Geology*, 191, 345-359.
367
- 368 Chen, Y. and Brantley, S.L. (2000) Dissolution of forsteritic olivine at 65°C and 2<pH<5.
369 *Chemical Geology* 165, 267-281.
370
- 371 Choukroun, M., Grasset, O., Tobie, G., Sotin, C. (2010) Stability of methane clathrate
372 hydrates under pressure: Influence on outgassing processes of methane on Titan. *Icarus*,
373 205, 581-593.
374
- 375 Diakonov, I., Pokrovski, G., Schott, J., Castet, S., Gout, R. (1996) An experimental and
376 computational study of sodium-aluminum complexing in crustal fluids. *Geochimica et*
377 *Cosmochimica Acta*, 60, 197-211.
378
- 379 Ehlmann, B. L., Mustard, J. F., Murchie, S. L. (2010) Geologic setting of serpentine
380 deposits on Mars, *Geophysical Research Letters*, 37, doi: 10.1029/2010GL042596.
381
- 382 Jamveit, B., Malthe-Sørensen, A., Kostenko, O. 2008. Reaction enhanced permeability
383 during retrogressive metamorphism. *Earth and Planetary Science Letters*, 267, 220-627.
384
- 385 Jons, N., Bach, W., Klein, F. (2010) Magmatic influence on reaction paths and element
386 transport during serpentinization. *Chemical Geology*, 274, 196-211.

387

388 Kelemen, P.B. and Matter, J. (2008) In situ carbonation of peridotite for CO₂ storage,
389 Proceedings of the National Academy of Sciences, 105, 17295-17300.

390

391 Kelemen, P.B. and Hirth, G. (2012). Reaction-driver cracking during retrograde
392 metamorphism: olivine hydration and carbonation. Earth and Planetary Science Letters,
393 345-348, 81-89.

394

395 Kerrick, D.M. (1990) The Al₂SiO₅ polymorphs. Reviews in Mineralogy, 22, 406 pp.

396

397 Klein, F., Bach, W., Jons, N., McCollom, T., Moskowitz, B., Berquo, T. (2009) Iron
398 partitioning and hydrogen generation during serpentinization of abyssal peridotites
399 from 15 degrees N on the Mid-Atlantic Ridge. Geochimica et Cosmochimica Acta, 73,
400 6868-6893.

401

402 Luquot, L., Andreani M., Godard, M., Gouze, P., and Gibert, B. (2010) Serpentinization of
403 sintered olivine during seawater percolation experiments. In : Water-Rock Interaction
404 XIII. Ed. by P. Birkle and I. S. Torres-Alvarado. London : Taylor & Francis.

405

406 Manning, C. (2006) Mobilizing aluminum in crustal and mantle fluids. Journal of
407 Geochemical Exploration, 89, 251-253.

408

409 Manning, C. (2007) Solubility of corundum + kyanite in H₂O at 700°C and 10 kbars:
410 evidence for Al-Si complexing at high pressure and temperature. Geofluids, 7, 258-269.

411

412 Marcaillou, C., Muñoz, M., Vidal, O., Parra, T., Harfouche, M. (2011) Mineralogical
413 evidences for H₂ degassing during serpentinization at 300°C/300 bars. Earth and
414 Planetary Science Letters, 303, 281-290.

415

416 Martin, B. and Fyfe, W. S. (1970) Some experimental and theoretical observations on the
417 kinetics of hydration reactions with particular reference to serpentinization, Chemical
418 Geology, 6, 185-195.

419

- 420 Martin, W., Baross, J., Kelley, D., Russel, M. (2008) Hydrothermal vents and the origin of
421 life. *Nature Review, Microbiology* 6, 805-814.
422
- 423 McCaig, A., Cliff, R.A., Escartin, J., Fallick, A.E., MacLeod, C.J. (2007) Oceanic detachment
424 faults focuses very large volumes of black smokers. *Geology*, 35, 935-938.
425
- 426 McCollom, T.M. and Seewald, J.S. (2007) Abiotic synthesis of organic compounds in deep-
427 sea hydrothermal environments. *Chemical Reviews*, 107, 382-401.
428
- 429 Muñoz, M., De Andrade, V., Vidal, O., Lewin, E., Pascarelli, S., Susini, J. (2006). Redox and
430 speciation micro-mapping using dispersive X-ray absorption spectroscopy: Application
431 to iron in chlorite mineral of a metamorphic rock thin section. *Geochemistry Geophysics*
432 *Geosystems*, 7, Q11020.
433
- 434 Nakamura, K. and Kato, Y. (2004) Carbonatization of oceanic crust by the seafloor
435 hydrothermal activity and its significance as a CO₂ sink in the Early Archean. *Geochimica*
436 *et Cosmochimica Acta* 68, 4595-4618.
437
- 438 Oger, P.M., Daniel, I., Picard, A. (2005). Development of a low-pressure diamond anvil
439 cell and analytical tools to monitor microbial activities in situ under controlled P and T.
440 *BBA Proteins Proteomics*, 1764, 434-442.
441
- 442 O'Hanley, D.S. and Dyar, M.D. (1993). The composition of lizardite 1T and the formation
443 of magnetite in serpentinites. *American Mineralogist*, 78, 844-844.
444
- 445 O'Hanley, D. S. (1996) *Serpentinites: Records of tectonic and petrological history*. Oxford
446 University Press.
447
- 448 Peacock, S.M. (1990) Fluid processes in subduction zones. *Science*, 258, 329-337.
449
- 450 Peacock, S.M. and Hyndman, R.D. (1999) Hydrous minerals in the mantle wedge and the
451 maximum depth of subduction thrust earthquakes. *Geophys. Res. Lett.*, 26:2517-2520.
452

- 453 Proskurowski, G., Lilley, M.D., Kelley, D.S., Olson, E.J. (2006) Low temperature volatile
454 production at the Lost City hydrothermal field, evidence from a hydrogen stable isotope
455 geothermometer. *Chemical Geology*, 229, 331-343.
456
- 457 Proskurowski, G., Lilley, M.D., Seewald, J.S., Fruh-Green, G.L., Olson, E.J., Lupton, J.E.,
458 Sylva, S.P., Kelley, D.S. (2008) Abiogenic hydrocarbon production at Lost City
459 hydrothermal field. *Science*, 319, 604-607.
460
- 461 Reynard, B., Hilaret, N., Balan, E., Lazzeri, M. (2007) Elasticity of serpentines and
462 extensive serpentinization in subduction zones. *Geophysical Research Letters*, 34, doi:
463 10.1029/2007GL030176.
464
- 465 Rudge, J.F., Kelemen, P.B., Spiegelman, M., 2010. A simple model of reaction-induced
466 cracking applied to serpentinization and carbonation of peridotite. *Earth and Planetary
467 Science Letters*, 291, 215-227.
468
- 469 Salvi, S., Pokrovski, G.S., Schott, J. (1998) Experimental investigation of aluminum-silica
470 aqueous complexing at 300°C. *Chemical Geology*, 151, 51-67.
471
- 472 Schrenk, M.O., Kelley, D.S., Baross, J.A., Delaney, J.R. (2004) Low archaeal diversity linked
473 to seafloor geochemical processes at the lost City Hydrothermal Field, Mid-Atlantic
474 Ridge. *Environmental Microbiology*, 6, 1086–1095.
475
- 476 Seyfried, W.E., Jr, Foustoukos, D.I., Fu, Q. (2007) Redox evolution and mass transfer
477 during serpentinization: An experimental and theoretical study at 200 °C, 500 bar with
478 implications for ultramafic-hosted hydrothermal systems at Mid-Ocean Ridges.
479 *Geochimica et Cosmochimica Acta*, 71, 3872–3886.
480
- 481 Seyfried, W.E., Pester, N.J., Ding, K., Rough, M. (2011) Vent fluid chemistry of the
482 Rainbow hydrothermal system (36°N, MAR) : phase equilibria and in situ pH controls on
483 seafloor alteration processes. *Geochimica et Cosmochimica Acta*, 75, 1574-1593
484

485 Solum, J.G., Hickman, S.H., Lockner, D.A., Moore, D.E., van der Pluijm, B.A., Schleicher,
486 A.M., Evans, J.P. (2006) Mineralogical characterization of protolith and fault rocks from
487 the SAFOD Main Hole. *Geophysical Research Letters*, 33,L21314.

488

489 Tomeoka, K. and Tanimura, I. (2000) Phyllosilicate-rich chondrule rims in the Vigarano
490 CV3 chondrite: Evidence for parent-body processes. *Geochimica et Cosmochimica Acta*,
491 64, 1971-1988.

492

493 Van der Lee, J., De Windt, L., Lagneau, V., Goblet, P. (2002) Presentation and application
494 of the reactive transport code CHESH-HYTEC, *Developments in Water Science*, 47, 599-
495 606.

496

497 Wegner, W.W. and Ernst, W.G. (1983) Experimentally determined hydration and
498 dehydration reaction rates in the system MgO-SiO₂-H₂O. *American Journal of Science*,
499 283-A, 151-180.

500

501

502 **Figure legends**

503

504 **Figure 1 : Optical images of the reaction progress in the lp-DAC.** Development with
505 time (A to D) of aluminous serpentine at the expense of olivine and Al₂O₃ microspheres
506 during experiment N°3a (Table1).

507

508 **Figure 2 : Monitoring reaction progress on the olivine grain with Raman**
509 **spectroscopy.** Example of reaction N°3a. Confocal Raman spectroscopy allows scanning
510 the olivine grain in depth. The time steps are those illustrated on Figure 1. The final
511 product of the reaction at t=47h is identified as amesite by comparison to the reference
512 spectrum from RUFF database. Olivine is the only mineral detected at t=0 and 2h. Then

513 Raman modes characteristic of amesite (arrows) are observed with relict olivine at
514 t=16h. Olivine is fully replaced by amesite at t=47h.

515

516 **Figure 3 : SEM and XRD characterization of the serpentine grains at the end of**
517 **reaction.** Example of Exp. N°3a. A) SEM image of the serpentine grains formed at the
518 expense of olivine. B) Zoom in of serpentine grains with EDS-SEM analysis of their mean
519 composition. C) XRD spectra of the serpentine grains with identification of the
520 characteristic peaks of serpentine minerals. No other phases are detected.

521

522 **Figure 4 : Comparison of the present results with serpentinization rates available**
523 **in the litterature.** Results of experiments N°1, 3a, 3b, 5, 6, realized with olivine grain
524 size ~100-150 μm , are plotted in comparison with the available data on serpentinization
525 rate of olivine or peridotite obtained under similar P-T conditions and grain size, i.e. 60-
526 80 μm (Martin and Fyfe 1970) and 105-150 μm (Wegner and Ernst 1983). Available
527 results obtained at lower P conditions (Luquot et al. 2010) and smaller grain sizes ~ 1
528 μm (Marcaillou et al. 2011) are also reported.

529

530

531

532

533

534

535

536

537

538 **Table 1 : Experimental conditions and main results**

Solid reactants 0.5 m NaCl in deionized H ₂ O pH _{init} (25°C)= 7 reacted at T=300°C , P=200 MPa	Duration (hours)	First serpentine grain (hours from start)	Reaction completion at the end
N°1 : Ol	168	No reaction observed	No
N°2 : Ol + Liz	182	No reaction observed	No
N°3 a : Ol + Al ₂ O ₃ b* : Ol + Al ₂ O ₃	119 144	2 (± 0.25) 2 (± 0.25)	Yes, completion at 48h (± 8) 65h (± 8)
N°4 : Ol + Al ₂ O ₃ + Liz	112	38 (±3)	No, reaction stopped or slowed down at t = 70h (±5)
Solid reactants 0.5 m NaCl in deionized H ₂ O pH _{init} (25°C)= 7 reacted at T=200°C , P=200 MPa			
N°5 : Ol + Al(OH) ₃ gel	70	1.5 (± 0.25)	Yes, completion at 45h (± 4)
N°6 : Ol + Al(OH) ₃ gel	50	1 (± 0.25)	Yes, completion at 37h (± 6)

539 *Experiment N°3b includes a first temperature step at 250°C for 3 days, that is not reported in the table, followed by a second and
 540 final step at 300°C for 6 days, reported in the table. No reaction was observed at 250°C since Al₂O₃ microspheres did not dissolve.
 541

542

543

544 **Figures**

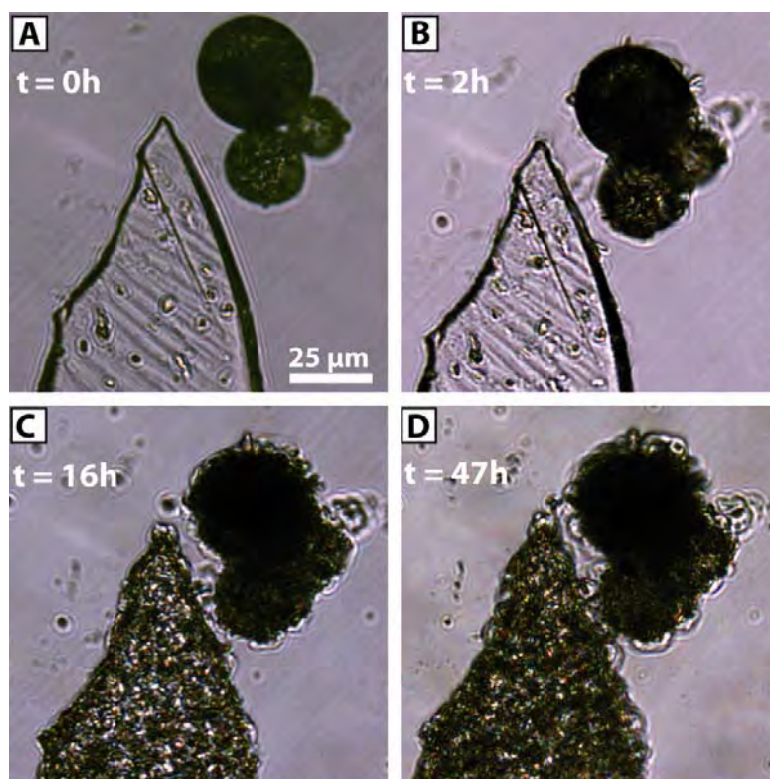


Figure 1

545

546

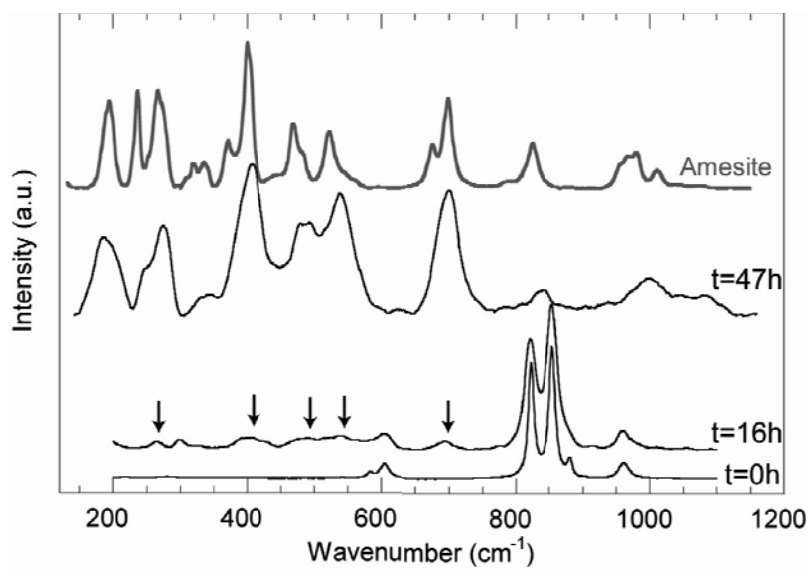


Figure 2

547

548

549

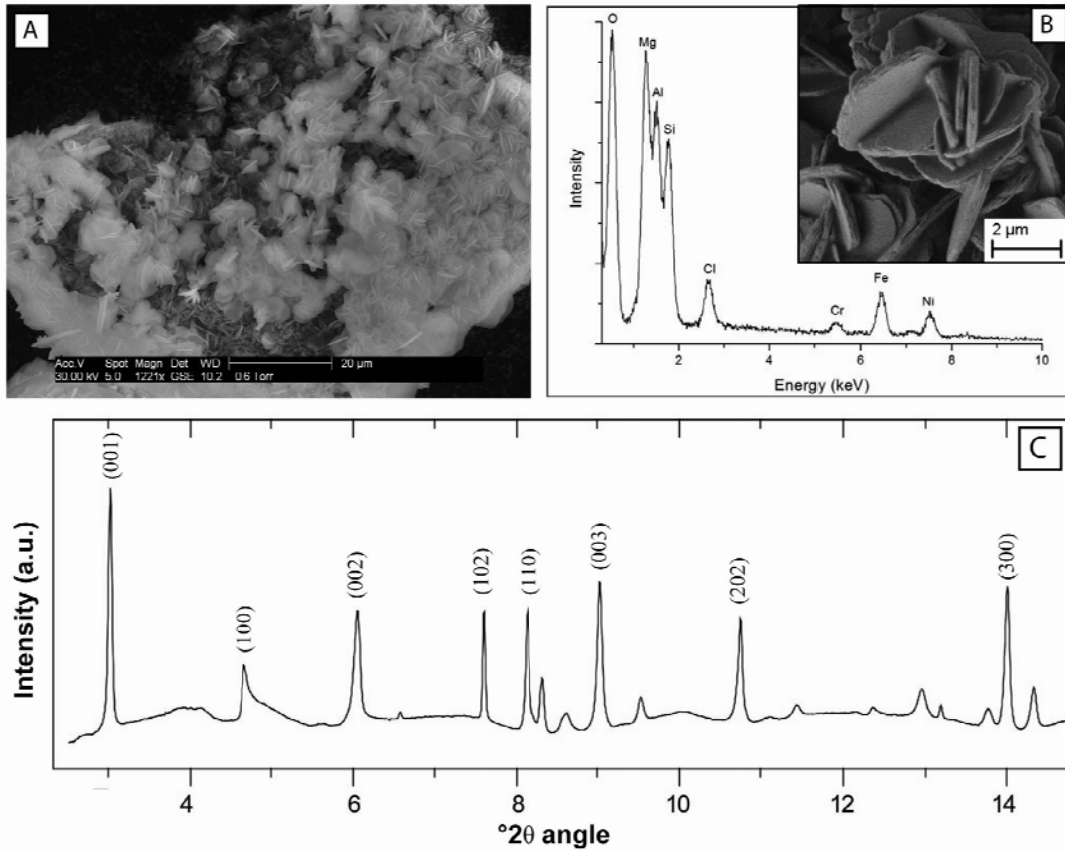


Figure 3

550

551

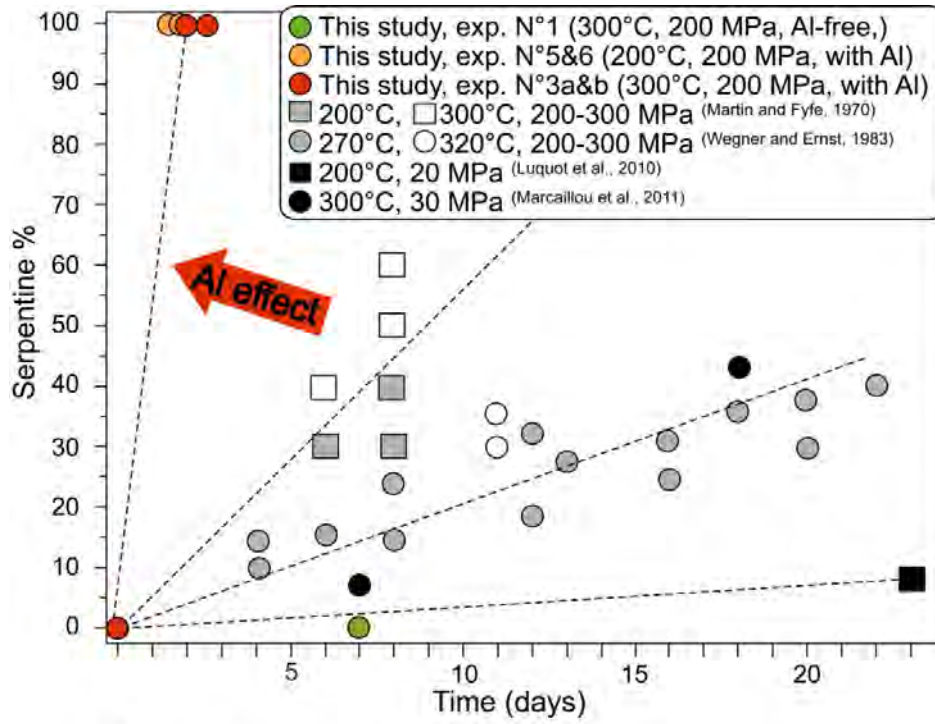


Figure4

552

553

554

555

556

557

558

559

560

561

562

563

564

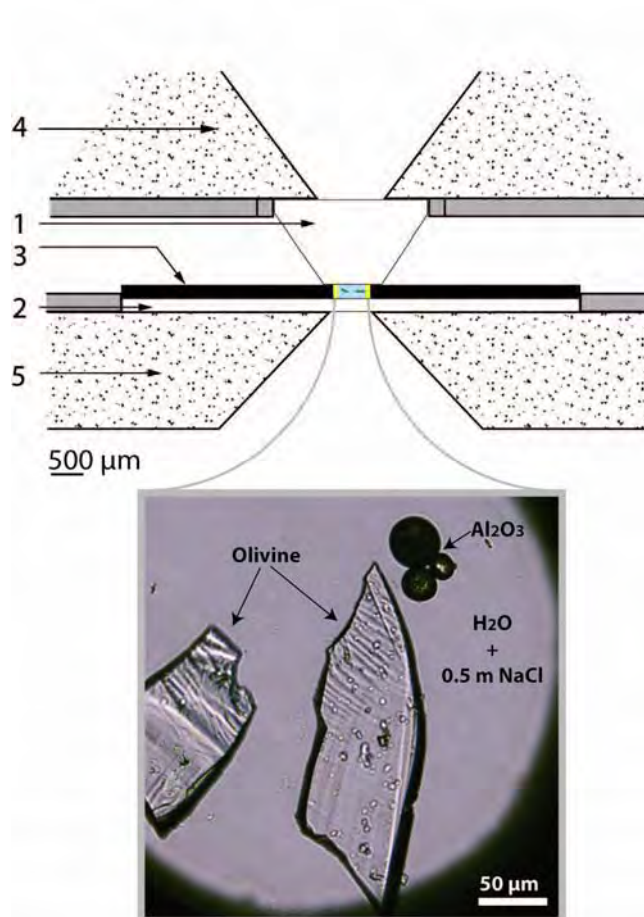
565

566

567 **SUPPORTING INFORMATION**

568

569 **Figures**



570

571 **Supporting Figure S1. Scheme of the low-pressure diamond anvil cell.** (1) diamond

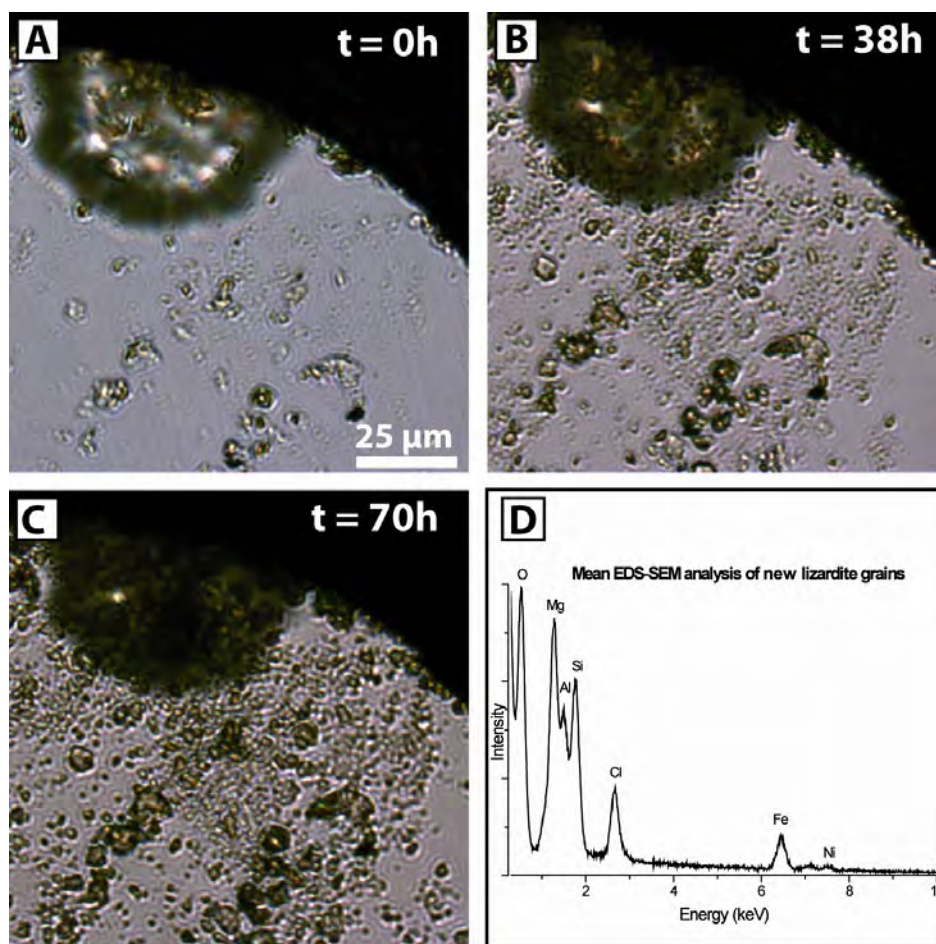
572 anvil, (2) diamond window, (3) Ni sample gasket lined with gold (inner diameter = 380

573 μm ; thickness = 300 μm), (4, 5) tungsten carbide seats. The experimental volume

574 (coloured in blue) is filled with reactants as illustrated by the optical image experiment

575 load N°3a at t=0. For more details on the lp-DAC, see Oger et al. (2005).

576



577

578 **Supporting Figure S2 : Optical images of the reacting cell.** Development with time of
579 serpentine at the expense of olivine and on initial lizardite nuclei during experiment N°4
580 (Table1).

581

582

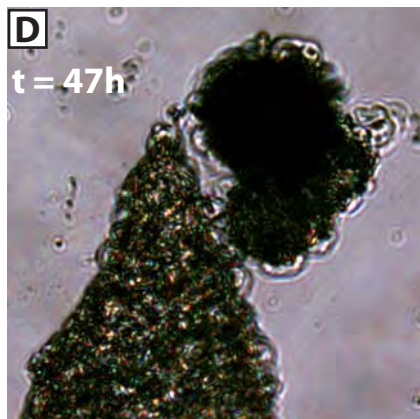
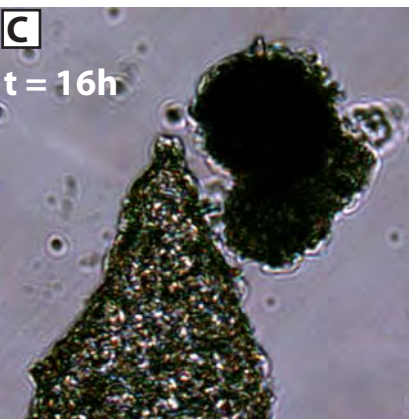
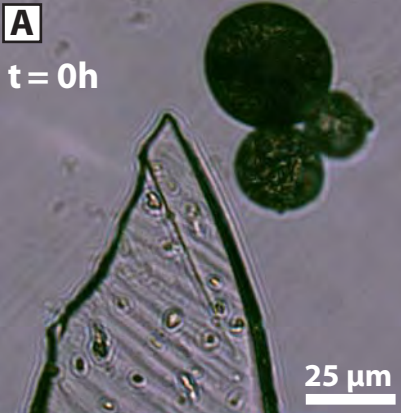


Figure 1

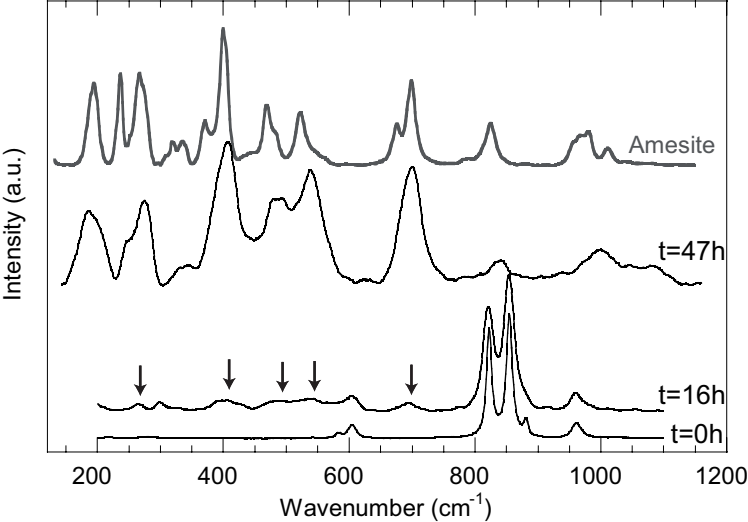


Figure 2

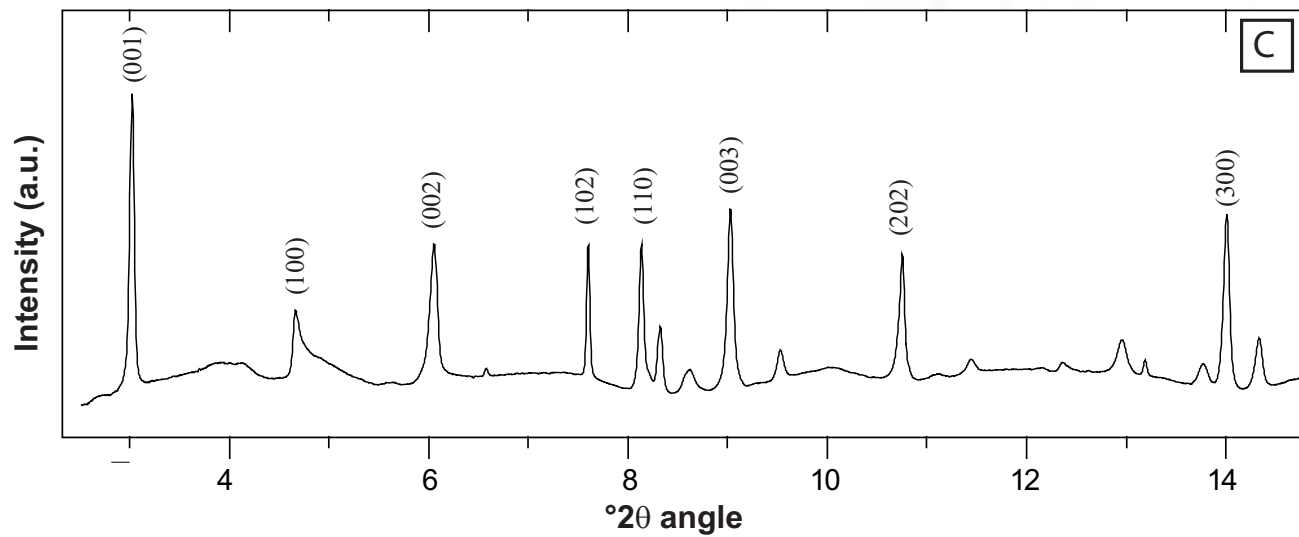
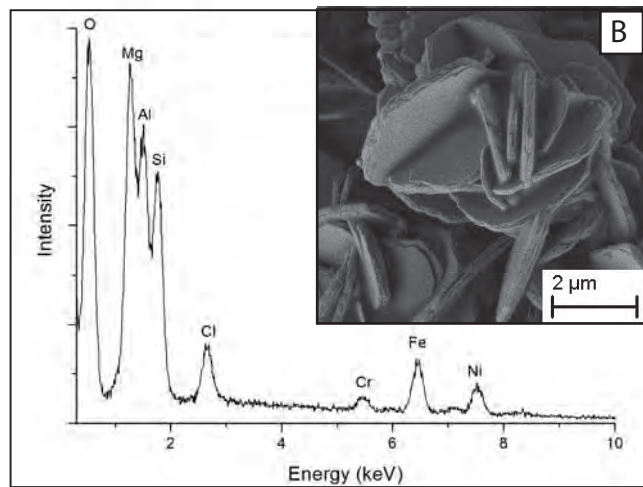
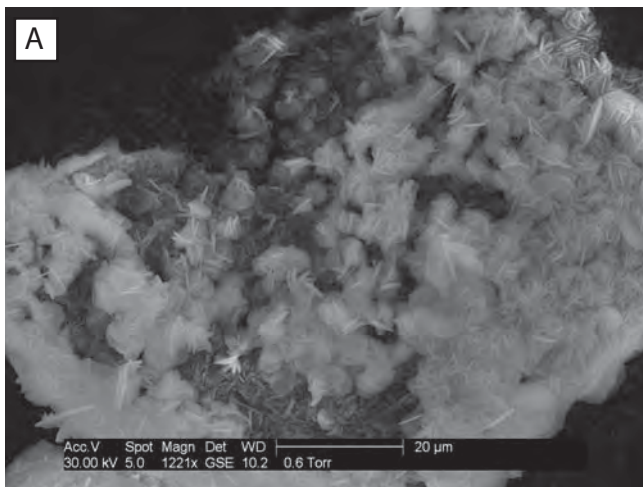


Figure 3

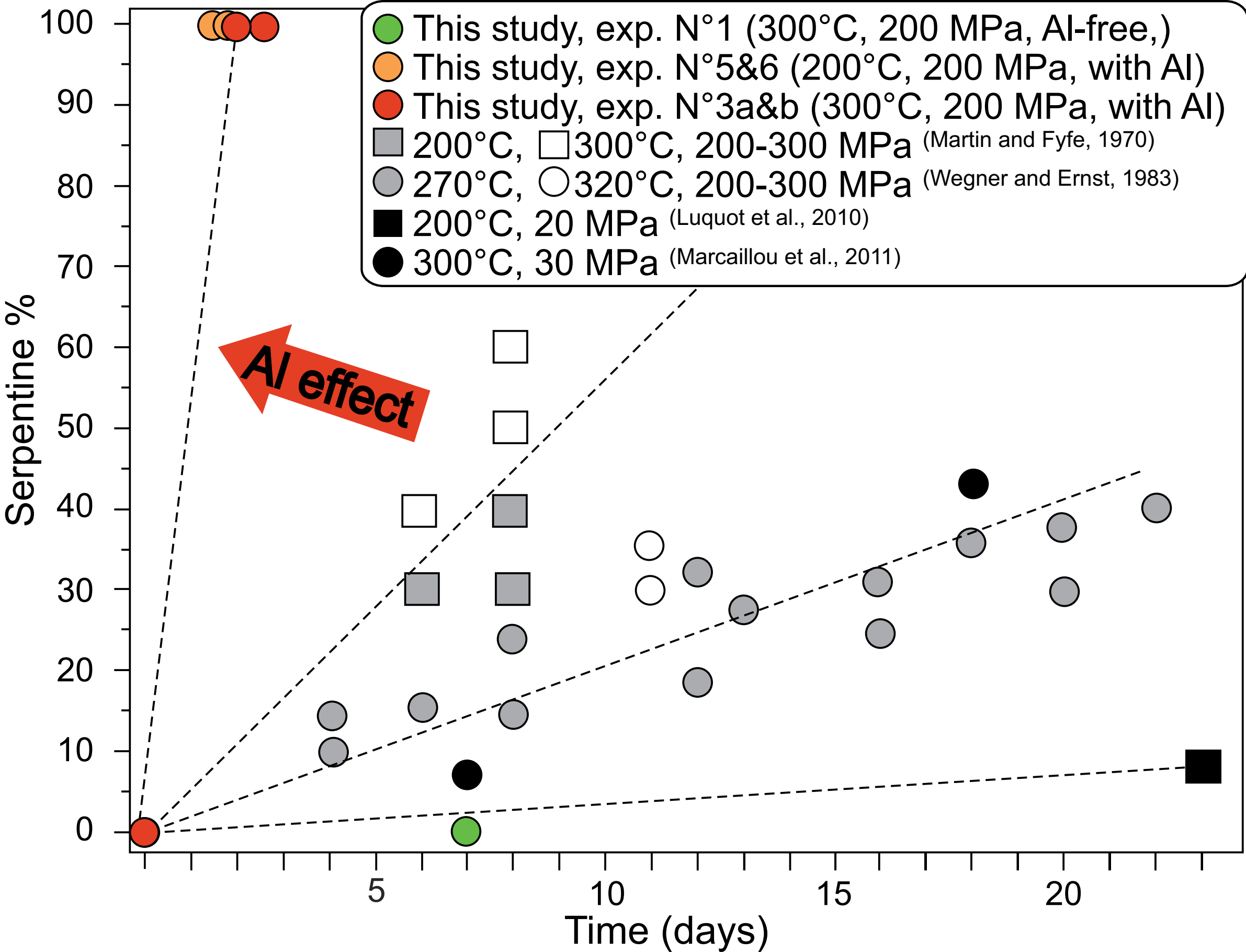


Figure4